Edge effects in an electrochemical reaction: HCOOH oxidation on a Pt ribbon

Jaeyoung Lee
Department of Environmental Science and Engineering, Gwangju Institute of Science and Technology, Gwangju 500-712, South Korea

Johannes Christoph, Taegeun Noh, Markus Eiswirth, and Gerhard Ertl
Fritz-Haber-Institut der Max-Planck-Gesellschaft, Faradayweg 4-6, D-14195 Berlin, Germany

(Received 21 November 2005; accepted 21 February 2007; published online 10 April 2007)

The use of a ribbon-shaped Pt electrode gives rise to edge effects of the interfacial potential, as is predicted from the potential theory in the form of the corresponding reaction-migration equation. They are studied in the bistable region of formic acid oxidation. Essentially, the edges tend to be more passive than the bulk of the electrode, which also causes a passivation (activation) transition to originate from the edges (center) of the ribbon. The experimental results are in agreement with simulations of the reaction-migration system. © *2007 American Institute of Physics*.
[DOI: 10.1063/1.2717163]

I. INTRODUCTION

There has been a resurgence of interest in the studies of the edge effect phenomena such as sharp point discharge by the rod of lightening protection, grain growth, and solidification of phase boundary, faster electrodeposition at edges of planar-shaped electrodes, and metal shrinkage from electrodissolution in various chemical and physical systems. All these phenomena can be reduced to the high (formally diverging) electric field at the edges of the electrodes, resulting in a high current density.

Up to now, many research groups have published relevant reports about edge effects in electrochemical systems,[1–3] but most were theoretical simulations, only a few studies of experimental observations were presented. In particular, there was no relevant reference of an experimental observation of the edge effect occurring in electrocatalysis (e.g., electro-oxidation of organic molecules).

Bistable media consisting of elements that have two steady states, which are stable under sufficiently small perturbations, are interesting systems of nonlinear electrochemistry. Sufficiently strong perturbations can cause transitions between these states. The fundamental form of a pattern in bistable media is a trigger wave, which represents a propagating front of transition from one stationary state into the other.[4–11] Strasser *et al.*[5] experimentally and theoretically demonstrated the bistability in formic acid oxidation on several different single crystalline Pt electrodes. Recently, Christoph *et al.*[4,6] presented the remote triggering of waves in electrochemical oxidation of a formic acid system under bistable conditions.

While on a ring electrode, investigated in the previous studies,[4,5,12–16] all locations are equivalent by symmetry, additional effects come into play on electrodes where this is not the case, i.e., when the symmetry of the ring is broken. Therefore, in this work a thin ribbon electrode will be studied, where points at the center are at a different state than points at the edges, which is expected to lead to spatially inhomogeneous stationary states of the bistable system, but should also have an impact on the spatiotemporal pattern formation. Recent relevant spatiotemporal data on a ribbon-shaped electrode under bistable systems are presented and compared with theoretical simulations developed by Christoph.[6]

II. THEORY

Since the mathematical derivation and theoretical calculations associated with the edge effect on ribbon electrode are similar to those on the disk electrode (which was already introduced by Christoph and Eiswirth[18]), only a brief mathematical description for a ribbon electrode will be given. An electrode with the length of L and the width of W is employed as the working electrode embedded in an insulator plane at $z=0$. The longer direction is the x axis, as shown in Fig. 1.

$$\tilde{x} \in [0,L], \quad \tilde{y} \in [-W/2, W/2]$$

$$\Rightarrow x \in [0,1]\ (0 \leqslant x \leqslant 1), \quad y \in [-b/2, b/2], \tag{1}$$

$$\text{with} \quad b \equiv W/L \leqslant 1, \quad A_{\mathrm{WE}} = L \times W,$$

where A_{WE} is the area of the working ribbon electrode and b is defined as W/L. The reference electrode (RE) is placed at a scaled distance of $\beta(\beta := d/L)$ in the center and on top of the working electrode (WE) with d being the horizontal physical distance between WE and RE.

Assuming the validity of the Laplace equation in the electrolyte $\Delta\Phi(x,y,z)=0$ for $z>0$, the boundary conditions for the potential distribution $\Phi(x,y,z)$ are given by the insulator

$$\delta\Phi/\delta z|_{z=0} = 0 \quad \text{for } (x,y) \notin \mathrm{WE},$$

together with the counterelectrode condition $\Phi=0$,

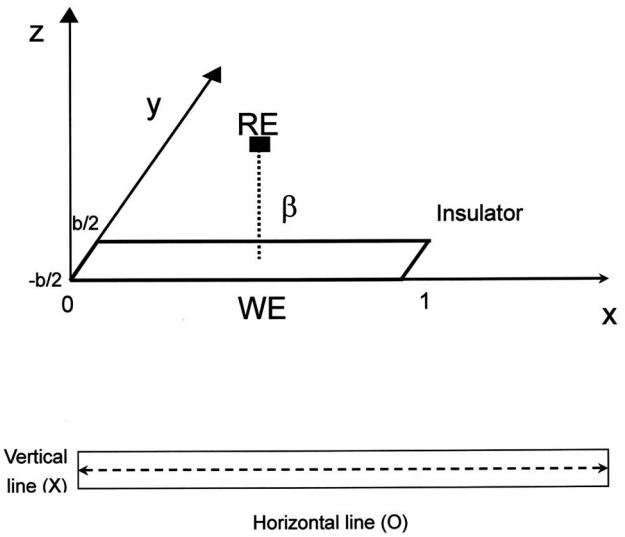

FIG. 1. Geometry of the ribbon working electrode with unit length and width b, embedded in an insulator plane. The reference electrode is placed at a distance of β.

$$\Phi = 0 \quad \text{for } x^2 + y^2 + z^2 \to \infty,$$

which is placed at infinity for reasons of mathematical simplicity, and the mixed boundary condition at the working electrode given by the current density balance of capacitive (i_{cap}), reaction (i_r), and migration current density (i_{mig}),

$$i_{\text{cap}} + i_r = i_{\text{mig}} \Rightarrow C_{\text{DL}} \delta u/\delta t + i_r = -\kappa\, \delta\Phi/\delta z|_{z=0} \quad \text{for } (x,y) \in \text{WE},$$

with $u(x,y,t)$ describing the double layer potential, C_{DL} represents the electrode capacitance, and the electrolyte conductivity is given by κ. These boundary conditions can be transformed into a reaction-migration equation using a Green's function[6,17,18]

$$\partial_t u(x,y,t) = -i_r(u,c) + \kappa h_{2D}(x,y)(E_0 - u) + \kappa \int_{-b/2}^{b/2} \int_0^1 H_{2D}(x,x',y,y')(u(x',y') - u(x,y))dx'dy',$$

where both the coupling function $H_{2D}(x,x',y',y)$ and the local function $h_{2D}(x,y)$ are explicitly position dependent, E_0 is the applied outer potential, and $c_i = c_i(x,y,t)$ are the relevant chemical concentrations at the electrode.

The inhomogeneity of the double layer potential is mainly decreasing along the y axis when the width b becomes smaller. Therefore, as b approaches 0, the inhomogeneity along the y axis diminishes, so we do not have to consider the change of the double layer potential along the y axis, because the pattern formation along this axis can be neglected. Therefore, when using a thin ribbon electrode with a small width, the spatiotemporal behavior of the double layer potential along the x-axis $u(x,t)$ can be described with a simpler reaction-migration equation [cf. Eq. (9) in Ref. 17],

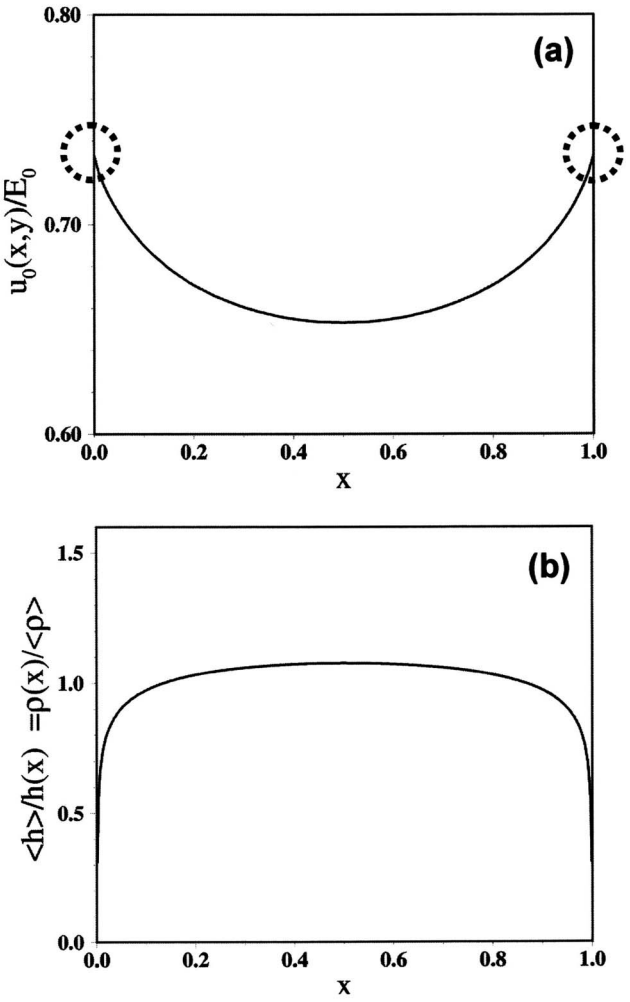

FIG. 2. (a) Double layer potential of a thin ribbon electrode (width $b = 0.01$) with a linear reaction current $i_r(u) = \mu u$, $E_0 = \kappa = \mu = 1$. The stationary double layer potential $u_0(x,y=0)$ is increasing towards the edges. Thus, the maximum of current density is obtained at the two edges ($x=0$ and 1). (b) The inverse of the local function $\langle h\rangle/h(x)$ of the coupling function equivalent to an effective local resistance $\rho(x)/\langle\rho\rangle$ [see Eq. (3)].

$$\partial_t u(x,t) = -i_r(u,c) + \kappa h(x)(E_0 - u) + \kappa \int_0^1 H_0(x,x')(u(x') - u(x))dx', \tag{2}$$

which is generally valid for all electrochemical systems. The mathematical derivation of these functions for a thin ribbon electrode is extensively described in Refs. 6 and 18. To further elucidate the edge effect, a local and average resistance can be defined according to the following equations:

$$\rho_{\text{ele}}(x) \equiv \frac{1}{\kappa h(x)}, \quad \rho_{\text{ele}}^M \equiv \frac{1}{\kappa \langle h(x)\rangle}, \tag{3}$$

where the higher current density towards the edges manifests itself in a lower local resistance, which vanished directly at the edges [Fig. 2(a)].

To fully describe the spatiotemporal dynamics at the double layer, suitable equations for the chemical concentrations are needed (as in Refs. 6, 13, 17, and 18). However, since the dynamics of the potential is much faster than the

chemical diffusion to the electrode, its gradual depletion can be neglected when observing potential trigger wave transitions or quasistationary states in the absence of oscillations. In addition, the reactant depletion can be prevented by stirring in the electrolyte. In both cases, the dynamics and the quasistationary states of the potential are obtained by keeping the concentration constant $c_i \approx c_{i0}$, so Eq. (2) reduces to

$$\partial_t u(x,t) = -i_r(u) + \frac{E_0 - u}{\rho_{\mathrm{ele}}(x)} + \kappa \int_0^1 H_0(x,x')(u(x') - u(x))dx'.$$

This reaction-migration equation may also be solely used in reactions where potential-dependent surface modifications are fast (as the OH formation in the formic acid reaction at higher potentials). Consequently, their coverage can be adiabaticaly incorporated into the reaction current, that is, $c_i = f_i(u)$, thus $i_r = i_r(u, f(u))$, often and in the case of the formic acid oxidation creating a nonmonotonous current-potential dependence and bistability.

Figure 2(b) shows the calculated stationary distribution $u_0(x)$ of the double layer potential at the central horizontal line of the ribbon electrode $u(x, y=0)$. The higher current density at the edges leads to a monotonously increasing potential towards the edges (marked with dotted circles), whereas the current and the average double layer potential $\langle u_0 \rangle$ are roughly given by solving the approximation equation $i_r(\langle u_0 \rangle) = (E_0 - \langle u_0 \rangle)/\rho_{\mathrm{ele}}^M$.

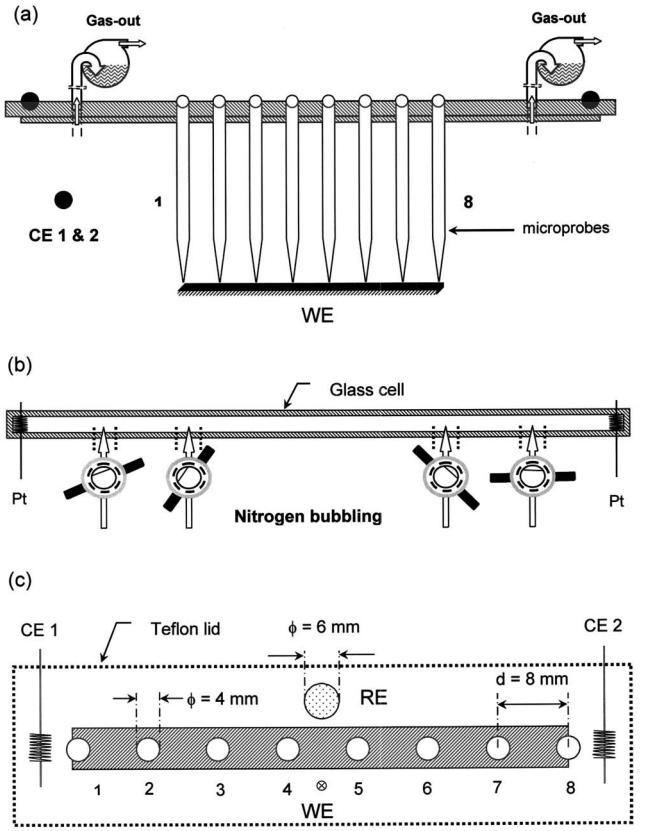

FIG. 3. Schematic diagram of an experimental setup for the investigation of the edge effect on a ribbon electrode. (a) Side view, (b) top view, and (c) detailed geometric drawing of the three electrodes used.

III. EXPERIMENT

Figure 3 shows the gas-tight, three-electrode, and one-compartment arrangement for the measurement of local potential distributions at electrochemical interfaces. The electrochemical cell body consisted of a glass cuboid capped with a Teflon lid holding all electrodes [see Fig. 2(a)]. A polycrystalline Pt ribbon with a length of 58.0 mm and with a width of 4.0 mm (thickness of 0.1 mm) was used as WE. Thus, the geometric area of the WE was 4.7 cm^2. Prior to each experiment, nitrogen bubbling was applied to remove the dissolved oxygen [see four gas inlet parts of Fig. 2(b)].

Two Pt coils with a thickness of 1 mm were used as counterelectrodes and placed far away from the WE ribbon electrode. The tip of a Luggin-Haber capillary hosting a $\mathrm{Hg/Hg_2SO_4}$, saturated $\mathrm{K_2SO_4}$ reference electrode was placed in the center of the ribbon WE. Eight reference electrodes were equally distributed at about 0.8 mm distance from the WE in order to monitor the local interfacial potential, as shown in Fig. 2(c).

All the solutions used in this section were prepared with ultrapure water (Millipore Milli-Q water, 18 MΩ cm). Chemical and electrochemical pretreatment and posttreatment of the ribbon working electrode were the same as that of the ring electrode (see Ref. 13) to confirm the absence of any residual surface impurities. The electrolyte was 0.1*M* HCOONa in 0.033*M* $\mathrm{H_2SO_4}$ (bulk solution *p*H=2.85).

An in-house-built potentiostat (ELAB of Fritz-Haber-Institut) was used for all cyclic voltammetry (CV) experiments and the data were transferred to an IBM compatible personal computer controlled by a general purpose interface bus (GPIB) interface.

IV. RESULTS AND DISCUSSION

Figure 4(a) shows a typical current-potential profile for HCOOH oxidation during the positive and negative direction scans on a polycrystalline Pt WE with a scan rate of 10 mV/s. The anodic peaks in the CV correspond to the oxidation of HCOOH in the course of both anodic and cathodic sweeps of the electrode potential. The fall of the current after the peak at +280 mV can be attributed to an increase in firmness of binding of the OH groups as the potential becomes more positive. This is associated with an increase in the OH coverage. On the cathodic scan, a sharp and significant current peak (burst) appears, attributed to the renewed oxidation of the fuel after removal of adsorbed OH. The small current at low potential is due to the poisoning of the surface by adsorbed CO.

Bistability of the current is obtained between +190 and +370 mV, which is subjected to the comparative study of inhomogeneous catalytic activity on the ribbon electrode on two different states, i.e., active state (*a*) on the positive scan and passive state (*p*) on the negative scan.

Figure 4(b) shows the stationary potential distribution along the Pt ribbon electrode in the electro-oxidation of HCOOH. These data were obtained in the bistable region on the anodic scan (a) and on the cathodic scan (b), as shown in

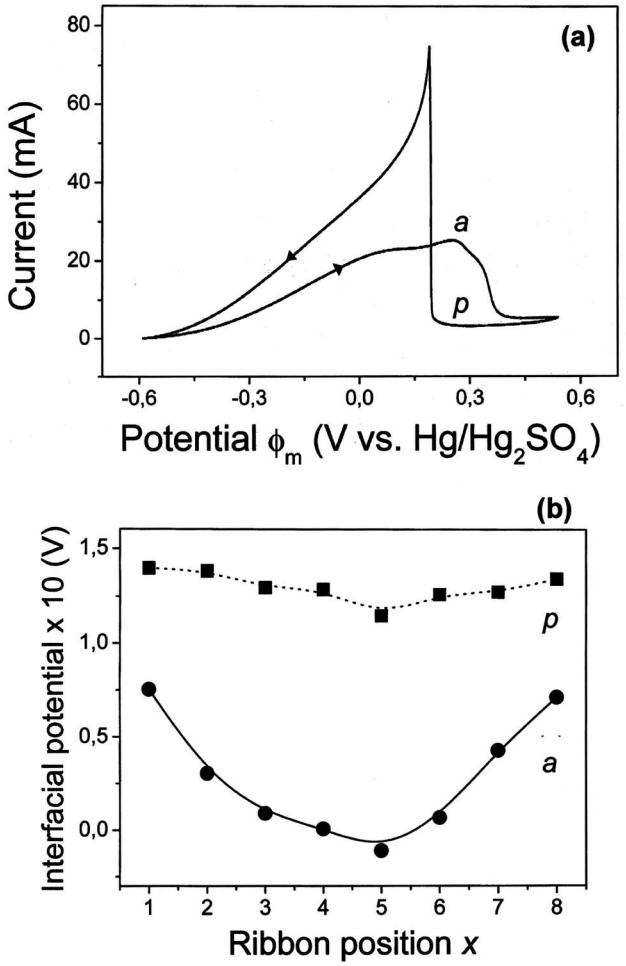

FIG. 4. Cyclic voltammetry of a polycrystalline Pt working electrode with a scan rate of 10 mV/s. *a* and *p* indicate the active state and the passive state, respectively. Experimental results of *bistability* at $\beta=0.7$. Fixed outer potential (E_0) is +290 mV. Eight microprobes were used in order to monitor the change of the double layer potential. Electrolyte is $0.1M$HCOONa/$0.033M$$H_2SO_4$. (i) Active state and (ii) passive state of bistable region.

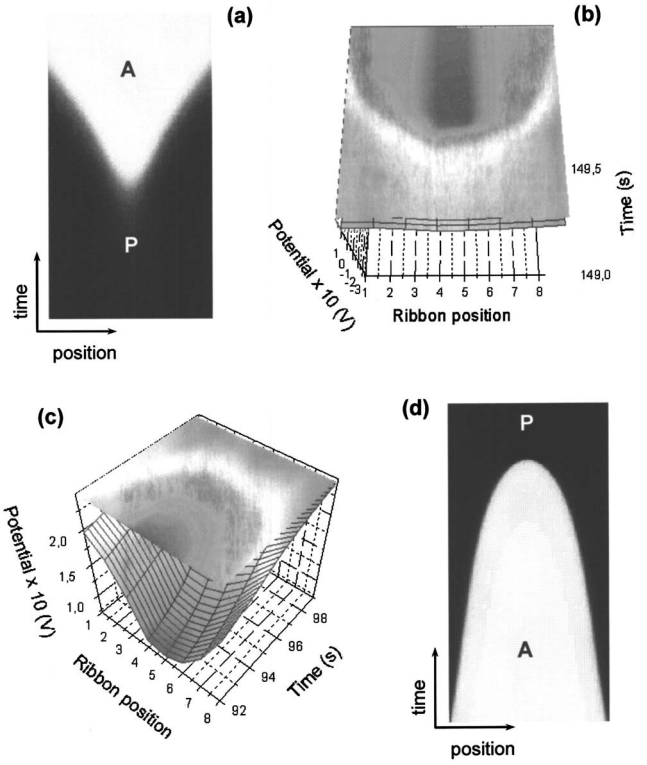

FIG. 5. Autonomous transition from passivation (*P*) to activation (*A*) on a thin ribbon electrode is shown. (a) Theoretical simulation (black: passive state, white: active state) using a suitable nonmonotonous reaction current $i_r(u)$ and (b) experimental observation (blue: active state, red: passive state). Autonomous transition from activation to passivation is shown. (c) Experimental data (blue: active state, red: passive state) and (d) theoretical simulation (black: passive state, white: active state).

Fig. 4(a). In this work, the RE was placed sufficiently far away from the WE (distance parameter $\beta=0.7$), so only the positive nonlocal coupling could occur.

As can be observed in Fig. 4(b), the higher current density (or lower local resistance) at the edges causes the electrode generally to be in a more passive state (higher interfacial potential) compared to the center. Furthermore, this edge effect is more pronounced in the active state, confirming the theoretical prediction that the homogeneity of the double layer potential distribution depends on the ratio of average double layer potential to the external outer potential $\langle u\rangle/E_0$.[6] Consequently, the active state (small $\langle u\rangle$) is more inhomogeneous than the passive state (larger $\langle u\rangle$).

The bistable region is terminated by autonomous transitions from the active to the passive state or vice versa. At low potential, activation fronts start from the middle of the ribbon electrode and propagate outwards, while passivation fronts at high potential always originated from the edges. Theoretical and experimental data of activation fronts are presented in Figs. 5(a) and 5(b), respectively. Note that the fronts are accelerated as the activated area increases, as commonly observed in bistable electrochemical systems.[19] In contrast, at the other end of the bistable region, observed on the anodic scan, passivation fronts started at both edges ($x=0$ and $x=1$) simultaneously and spread until they met at the center. Figures 5(c) and 5(d) reproduce experimental observation and theoretical simulation of autonomous passivation phenomena in bistable systems. Again the front velocity increases as the fronts spread.

V. CONCLUSIONS

Due to electrostatic effects, the edges of an electrode tend to be more passive (i.e., exhibit higher interface potential) than the bulk areas. Consequently, passivation (activation) fronts in the bistable regime originate from the edges (center).

[1] D. K. Cope, J. Electroanal. Chem. **439**, 7 (1997).
[2] K. B. Oldham, J. Electroanal. Chem. **420**, 53 (1997).
[3] N. K. Simha and K. Bhattacharya, Mater. Sci. Eng., A **273–275**, 241 (1999).
[4] J. Christoph, P. Strasser, M. Eiswirth, and G. Ertl, Science **284**, 291 (1999).
[5] P. Strasser, J. Christoph, W.-F. Lin, M. Eiswirth, and J. L. Hudson, J. Phys. Chem. A **104**, 1854 (2000).
[6] J. Christoph, Ph.D. thesis, Freie Universität Berlin 1999 (http://www.diss.fu-berlin.de/2000/11/).
[7] R. Luther, Z. Elektrochem. **12**, 596 (1906); reprinted in J. Chem. Educ. **64**, 1995 (1987).

[8] P. Fischer, Ann. Eugenics **7**, 335 (1937).
[9] Ya. B. Zeldovich and D. A. Frank-Kamenetskii, Zh. Fiz. Khim. **12**, 100 (1938).
[10] R. Kapral and K. Showalter, *Chemical Waves and Patterns* (Kluwer, Dordrecht, 1995).
[11] Physica D **49**, 1 (1991), special issue on wave patterns in chemical and biological systems, edited by H. L. Swinney and V. I. Krinsky.
[12] P. Grauel, J. Christoph, G. Flätgen, and K. Krischer, J. Phys. Chem. **102**, 10264 (1998).
[13] J. Lee, J. Christoph, P. Strasser, M. Eiswirth, and G. Ertl, J. Chem. Phys. **115**, 1485 (2001).
[14] H. Varela and K. Krischer, J. Phys. Chem. B **106**, 12258 (2002).
[15] J. Lee, J. Christoph, M. Eiswirth, and G. Ertl, Chem. Phys. Lett. **346**, 246 (2001).
[16] P. Grauel, H. Varela, and K. Krischer, Faraday Discuss. **120**, 165 (2001).
[17] J. Christoph, R. Otterstedt, M. Eiswirth, N. Jaeger, and J. L. Hudson, J. Chem. Phys. **110**, 8614 (1999).
[18] J. Christoph and M. Eiswirth, Chaos **12**, 215 (2002).
[19] G. Flätgen and K. Krischer, Phys. Rev. E **51**, 3997 (1995).